

Tunable van Hove Singularity without Structural Instability in Kagome Metal CsTi₃Bi₅

Bo Liu,^{1,*} Min-Quan Kuang^{2,*} Yang Luo,^{1,*} Yongkai Li,^{3,4,*} Cheng Hu⁵, Jiarui Liu,^{1,6} Qian Xiao,⁷ Xiquan Zheng,⁷ Linwei Huai,¹ Shuting Peng,¹ Zhiyuan Wei,¹ Jianchang Shen¹, Bingqian Wang,¹ Yu Miao,¹ Xiupeng Sun,¹ Zhipeng Ou,¹ Shengtao Cui,⁸ Zhe Sun,⁸ Makoto Hashimoto,⁹ Donghui Lu,⁹ Chris Jozwiak¹⁰, Aaron Bostwick¹⁰, Eli Rotenberg¹⁰, Luca Moreschini^{5,11}, Alessandra Lanzara,^{5,11} Yao Wang,⁶ Yingying Peng⁷,

Yugui Yao,^{3,4} Zhiwei Wang,^{3,4,12,‡} and Junfeng He^{1,†}

¹Department of Physics and CAS Key Laboratory of Strongly-coupled Quantum Matter Physics, University of Science and Technology of China, Hefei, Anhui 230026, China

²Chongqing Key Laboratory of Micro & Nano Structure Optoelectronics, and School of Physical Science and Technology, Southwest University, Chongqing 400715, China

³Centre for Quantum Physics, Key Laboratory of Advanced Optoelectronic Quantum Architecture and Measurement (MOE), School of Physics, Beijing Institute of Technology, Beijing 100081, China

⁴Beijing Key Lab of Nanophotonics and Ultrafine Optoelectronic Systems, Beijing Institute of Technology, Beijing 100081, China

⁵Material Sciences Division, Lawrence Berkeley National Laboratory, Berkeley, California 94720, USA

⁶Department of Physics and Astronomy, Clemson University, Clemson, South Carolina 29631, USA

⁷International Center for Quantum Materials, School of Physics, Peking University, Beijing 100871, China

⁸National Synchrotron Radiation Laboratory, University of Science and Technology of China, Hefei, Anhui 230026, China

⁹Stanford Synchrotron Radiation Lightsource, SLAC National Accelerator Laboratory, Menlo Park, California 94025, USA

¹⁰Advanced Light Source, Lawrence Berkeley National Laboratory, Berkeley, California 94720, USA

¹¹Department of Physics, University of California, Berkeley, Berkeley, California 94720, USA

¹²Material Science Center, Yangtze Delta Region Academy of Beijing Institute of Technology, Jiaxing 314011, China



(Received 12 December 2022; revised 24 March 2023; accepted 5 June 2023; published 12 July 2023)

In kagome metal CsV₃Sb₅, multiple intertwined orders are accompanied by both electronic and structural instabilities. These exotic orders have attracted much recent attention, but their origins remain elusive. The newly discovered CsTi₃Bi₅ is a Ti-based kagome metal to parallel CsV₃Sb₅. Here, we report angle-resolved photoemission experiments and first-principles calculations on pristine and Cs-doped CsTi₃Bi₅ samples. Our results reveal that the van Hove singularity (vHS) in CsTi₃Bi₅ can be tuned in a large energy range without structural instability, different from that in CsV₃Sb₅. As such, CsTi₃Bi₅ provides a complementary platform to disentangle and investigate the electronic instability with a tunable vHS in kagome metals.

DOI: 10.1103/PhysRevLett.131.026701

Kagome metals AV₃Sb₅ (A = K, Rb, Cs) have attracted much interest due to the coexistence of multiple exotic orders and states, ranging from superconductivity [1–3], charge density wave (CDW) [4–12], pair density wave [12], stripe order [4], nematic order [13,14], topologically non-trivial states [1,15], and time-reversal symmetry breaking states [11,16–18]. Despite the richness of these phenomena, their underlying mechanisms are still under debate. In principle, either electronic or structural instabilities of a material can drive the system into an ordered state with a lower energy. In AV₃Sb₅, electronic instabilities are naturally provided by van Hove singularities (vHSs) in the electron dispersion [19–22], and the structural instabilities are evidenced by the imaginary frequency in the phonon dispersion [23]. As a result, the explanations of the experimentally identified orders are often controversial. For example, the CDW order in AV₃Sb₅ has been attributed to either electronic nesting between vHSs [22–25] or

electron-phonon coupling [26–30]; the rotational symmetry breaking has been associated with either electronic nematicity [13,14,31] or lattice modulation [14,31]. The coexisted instabilities in both electron and lattice degrees of freedom make it very challenging to identify the primary driving mechanism for the various orders in AV₃Sb₅. In this regard, the importance of comparative studies in a parallel material system is clear. Theoretical calculations have predicted dozens of materials, which are similar to AV₃Sb₅ [32,33]. However, ATi₃Bi₅ (A = Cs, Rb) is the only material family that has been successfully synthesized recently [34,35].

In this Letter, we investigate pristine and Cs surface doped CsTi₃Bi₅ samples by angle-resolved photoemission spectroscopy (ARPES) measurements and first-principles calculations. The band structure of CsTi₃Bi₅ is clearly revealed. It shows a clear resemblance to the calculated result. The vHS is well above Fermi level (E_F) in the

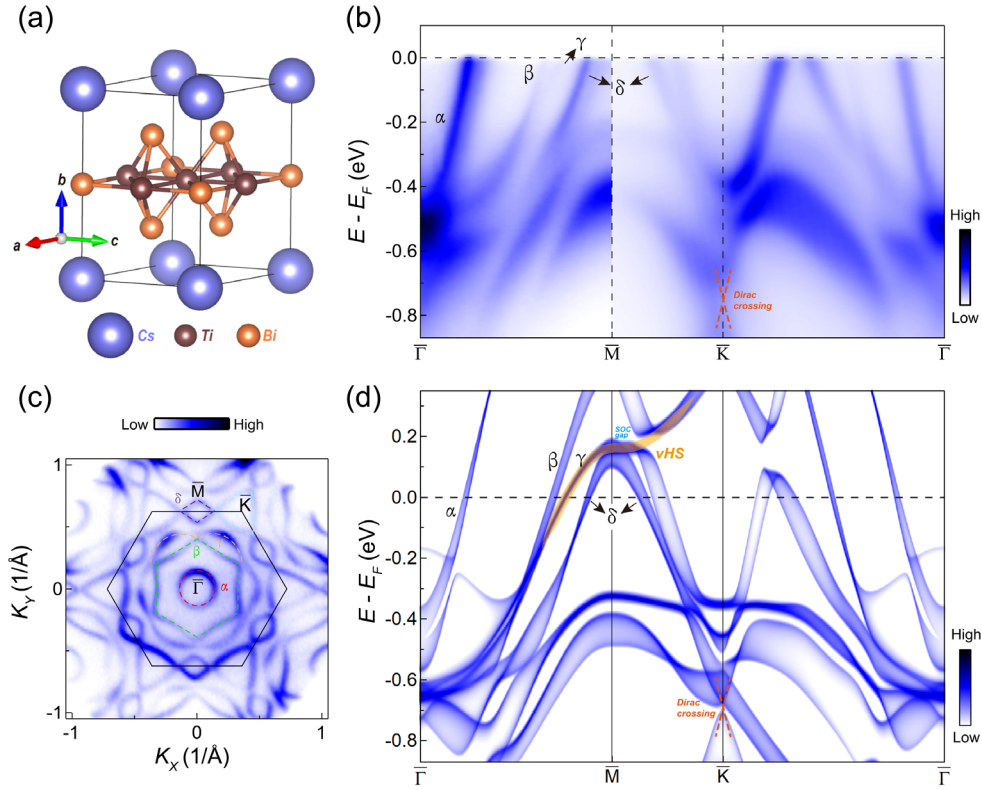


FIG. 1. Electronic structure of CsTi₃Bi₅. (a) Crystal structure of CsTi₃Bi₅. (b)–(c) Photoelectron intensity plot of the band structure along the $\bar{\Gamma}$ - \bar{M} - \bar{K} - $\bar{\Gamma}$ direction (b) and the Fermi surface (c) of CsTi₃Bi₅ measured with 78 eV photons at 7 K. The dashed lines in (c) are a guide to the eye for the different Fermi surface sheets. (d) The bulk band structure of CsTi₃Bi₅ obtained from first-principles calculations with spin-orbit coupling included. The electronlike band around $\bar{\Gamma}$ and the holelike bands near \bar{M} are labeled as α , β , γ , and δ band, respectively. The orange shade is a guide to the eye for the vHS.

pristine CsTi₃Bi₅. Surprisingly, the position of the vHS can be easily tuned in a large energy range by Cs surface doping. This property is distinct from that in CsV₃Sb₅, where the Cs surface doping primarily changes the electronlike band formed by Sb orbitals but has little effect on the vHS formed by V orbitals [36]. First-principles calculations further reveal the absence of structural instability in both pristine and electron doped CsTi₃Bi₅. This is also confirmed by our low-temperature x-ray diffraction measurements on the CsTi₃Bi₅ sample. As such, our results establish CsTi₃Bi₅ as a complementary material platform to CsV₃Sb₅, in which the electronic instability can be systematically examined without the interference from the lattice degree of freedom. These studies also provide new insights on the origin of CDW order and nematic order in the related kagome metals.

Single crystals of CsTi₃Bi₅ were grown by a self-flux method with binary Cs-Bi as the flux. The raw materials were loaded in an alumina crucible and sealed in an evacuated quartz tube. The tube was heated slowly to 1000 °C and held for 12 h. It was then cooled down to 850 °C at a rate of 10 °C/h and to 500 °C at a rate of 3 °C/h, at which the flux was removed by a centrifuge. The synchrotron-based ARPES measurements were performed

at Advanced Light Source (ALS) beamline 7.0.2 and Stanford Synchrotron Radiation Lightsources (SSRL) beamline 5-2, with some preliminary tests at National Synchrotron Radiation Laboratory. ARPES measurements were also carried out at our lab-based ARPES system using 21.2 eV photons with a total energy resolution of ~ 5 meV and a base pressure of better than 5×10^{-11} torr. The Fermi level was determined by measuring a polycrystalline Au piece in an electrical contact with the samples. First-principles calculations were performed by using the VASP software package. The details of the calculations and the related parameters are described in the Supplemental Material [37].

The crystal structure of CsTi₃Bi₅ is similar to that of CsV₃Sb₅ [Fig. 1(a)]. The Ti sublattice forms a kagome net, which is interwoven with a hexagonal net of Bi atoms in the same plane. The measured band structure of CsTi₃Bi₅ is shown in Fig. 1(b), which bears a clear resemblance to that of the first-principles calculations [Fig. 1(d)]. Because of the layered nature of the material, a projected in-plane Brillouin zone (BZ) is used for the description. The electronic structure near the $\bar{\Gamma}$ point is dominated by an electronlike band (labeled as the α band, hereafter), giving rise to a circular Fermi surface sheet [Fig. 1(c)]. Multiple

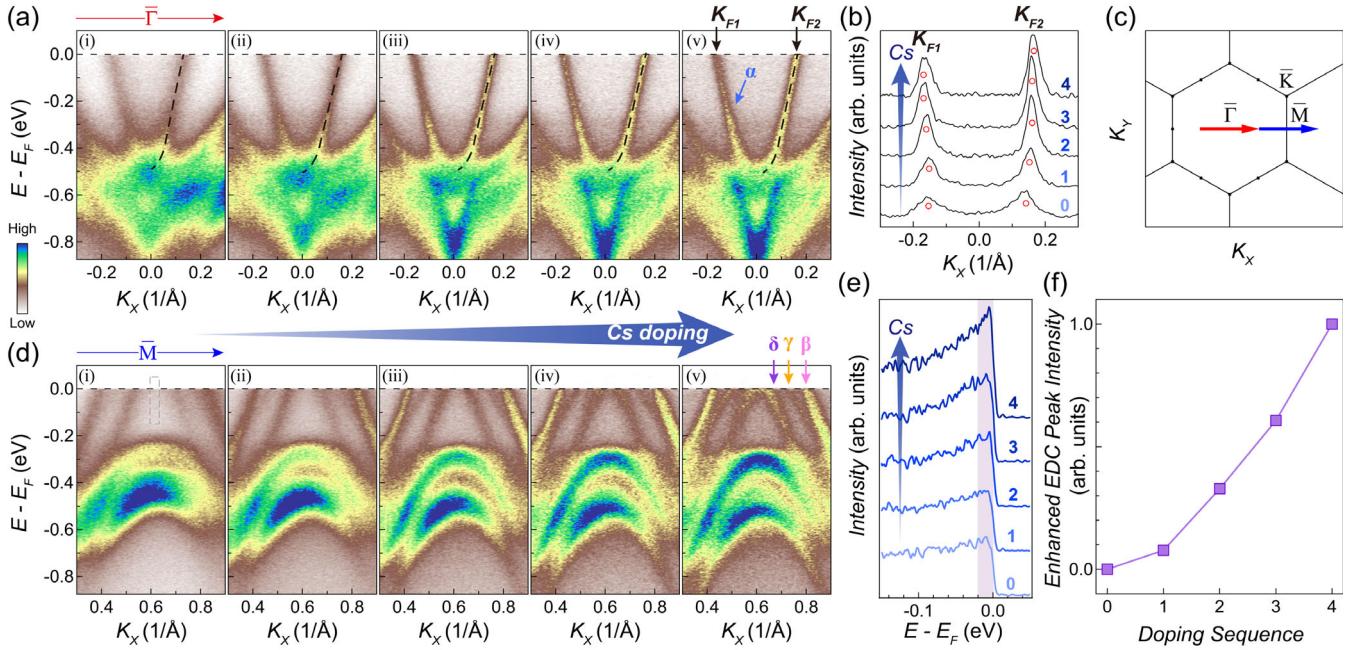


FIG. 2. Evolution of the electronic structure with Cs surface doping at 7 K. (a) Photoelectron intensity plot of the band structure around $\bar{\Gamma}$ (along the \bar{M} - $\bar{\Gamma}$ - \bar{M} direction) as a function of continuous Cs doping on the same sample, measured with 21.2 eV photons. The results at doping sequences 0–4 are shown in (i)–(v), respectively. Doping sequence 0 indicates the pristine CsTi₃Bi₅ sample. The dashed lines are a guide to the eye. (b) Momentum distribution curves (MDCs) at E_F extracted from (a). The numbers 0–4 denote the doping sequences. (c) The projected in-plane BZ and the momentum locations of the cuts. (d) Same as (a), but for the band structure around \bar{M} (along the $\bar{\Gamma}$ - \bar{M} - $\bar{\Gamma}$ direction). (e) Integrated EDC around the \bar{M} point in (d). The integration window is marked by the gray dashed box in the first panel of (d). The numbers 0–4 denote the doping sequences. (f) Enhanced EDC peak intensity around \bar{M} as a function of the doping sequence. The absolute EDC peak intensity at the doping sequence x ($x = 0$ –4) is calculated by integrating the area between -20 meV and E_F [the pink shaded region in (e)] of the corresponding EDC, and labeled as I_x . The enhanced EDC peak intensity is defined as $(I_x - I_0)/(I_4 - I_0)$.

holelike bands are observed around the \bar{M} point, which are labeled as the β , γ , and δ band, respectively [Figs. 1(b), 1(d)]. We note that the β and γ bands are very close to each other below E_F [Fig. 1(b)], which can be better resolved when they are well separated in the doped sample [Fig. 2(d)]. These holelike bands are associated with the hexagonal, flowerlike and diamondlike Fermi surface sheet, respectively [Fig. 1(c)]. A Dirac-like crossing can be seen at the \bar{K} point well below E_F [Figs. 1(b), 1(d)]. A triangular Fermi surface sheet is observed around the \bar{K} point [Fig. 1(c)]. The characteristic vHS of the kagome lattice is shown at \bar{M} point in the calculation [Fig. 1(d), indicated by the orange shade, the small energy gap is induced by the spin-orbit coupling]. Nevertheless, the vHS is located at ~ 150 meV above E_F , which cannot be probed by the photoemission measurements [Fig. 1(d)].

After revealing the overall electronic structure of the CsTi₃Bi₅, we now investigate the doping evolution via *in situ* surface deposition of Cs atoms. As shown in Fig. 2(a), the electronlike band (α band) around $\bar{\Gamma}$ exhibits a moderate change as a function of Cs doping. The bottom of the band shows a little movement in energy (also see Supplemental Material Fig. S1 [37]). The distance between two Fermi momenta of this band (k_{F1} and k_{F2}) increases slightly with

doping [Figs. 2(a), 2(b)]. On the contrary, the energy bands around the \bar{M} point exhibit more significant changes as a function of the Cs doping [Fig. 2(d), Supplemental Material, Fig. S1 [37]]. In particular, the γ and δ bands present a clear downward shift, echoing the expected electron doping with Cs surface deposition. We note that the top of these holelike bands starts to appear with sufficient Cs doping [Fig. 2(d)(v)], indicating that the vHS is in the vicinity of E_F . This is also evidenced by the enhanced electron density of states at E_F in this momentum region [Figs. 2(e), 2(f)]. The integrated energy distribution curve (EDC) around the \bar{M} point shows a negligible peak in the pristine CsTi₃Bi₅ [Fig. 2(e), doping sequence 0], as the vHS is well above E_F [Fig. 2(d)(i)]. However, the peak intensity increases significantly with Cs doping, demonstrating the boost of low energy electron density of states as the vHS approaches E_F [Figs. 2(e), 2(f)]. In order to quantitatively unveil the vHS, the Cs surface doping is reproduced at an elevated temperature ($T = 200$ K), where the thermal population of electrons enables a complete examination of the fine features around E_F . As shown in Figs. 3(a)–3(d), the vHS is indeed shifted downward with the Cs doping. On the sufficiently doped sample, the flat dispersion of the vHS can be clearly identified in the vicinity of E_F [Figs. 3(b), 3(d), also see

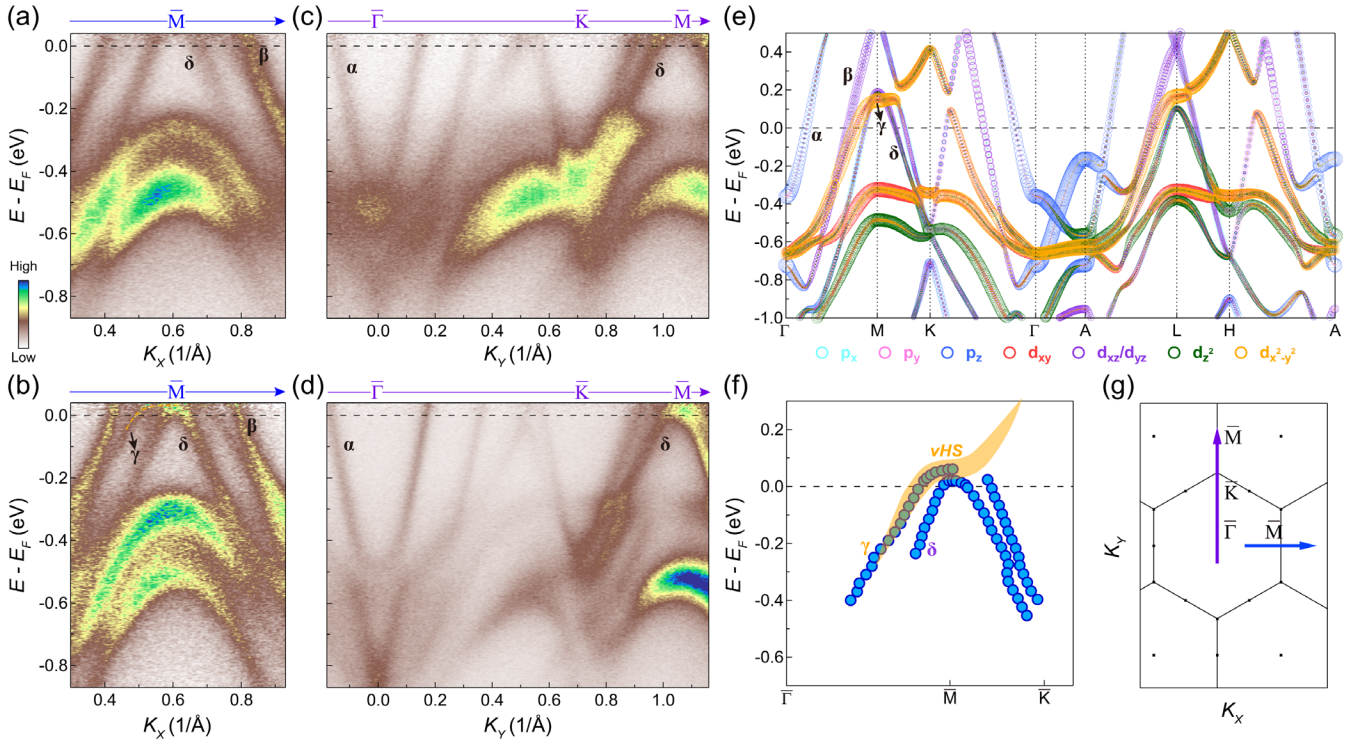


FIG. 3. Doping evolution of the vHS. (a)–(b) Photoelectron intensity plot of the band structure around \bar{M} (along the $\bar{\Gamma}$ – \bar{M} – $\bar{\Gamma}$ direction) before (a) and after (b) the Cs surface doping, measured with 21.2 eV photons at 200 K. (c)–(d) Same as (a)–(b), but measured along the $\bar{\Gamma}$ – \bar{K} – \bar{M} direction. (e) Orbital-resolved band structure obtained by first-principles calculations. Different orbitals are presented in different colors. The size of the markers represents the spectral weight of the orbitals. (f) Quantified dispersion of the γ and δ bands near \bar{M} after the sufficient Cs doping, extracted from (b) and (d). The orange shade is a guide to the eye for the vHS. (g) The projected in-plane BZ and the momentum locations of the cuts.

Supplemental Material, Figs. S2 and S3 [37]). These results are quantitatively extracted from the raw data and summarized in Fig. 3(f). Orbital-resolved calculations have also been carried out, which illustrate that the electronlike α band around $\bar{\Gamma}$ is dominated by Bi P_z orbital, whereas the vHS is primarily associated with Ti $d_{x^2-y^2}/d_{xy}$ orbital [Fig. 3(e)]. These observations have collectively depicted an integrated picture of orbital selective movements of the energy bands with Cs doping—the vHS with Ti d orbitals can be tuned in a large energy range, whereas the electronlike α band with Bi P orbitals remains less sensitive to the doping process. This is distinct from the evolution in CsV_3Sb_5 , where the vHS with V d orbitals shows little change with Cs surface doping, but the electronlike band with Sb P orbitals shifts ~ 240 meV in energy [36].

Next, we examine the lattice degree of freedom in the CsTi_3Bi_5 crystal. In CsV_3Sb_5 , both Star of David (SD) and inverse Star of David (ISD) structures are considered to be more stable than the kagome lattice. Therefore, we have followed the idea in CsV_3Sb_5 [23], and calculated the change of total energy in CsTi_3Bi_5 , assuming that the lattice is breathing in and out towards the potential SD and ISD structures [Fig. 4(a)]. Similar to the earlier report, either SD or ISD structure shows a lower total energy than that of the kagome structure in CsV_3Sb_5 [Fig. 4(b)], leading

to structural instabilities of the material [23]. On the contrary, the kagome structure in CsTi_3Bi_5 exhibits the lowest total energy, demonstrating the absence of structural instability [Fig. 4(c)]. This result remains solid when electron doping is considered in the CsTi_3Bi_5 system [Fig. 4(d)]. Phonon spectra are also calculated for both pristine and electron doped CsTi_3Bi_5 [Fig. 4(e)]. The absence of imaginary frequency echoes a stable kagome structure in CsTi_3Bi_5 . In addition, we have carried out low-temperature x-ray diffraction measurement on CsTi_3Bi_5 [Fig. 4(f)], which also confirms the kagome structure without any supermodulation of the lattice.

Finally, we discuss the implications of our observations. The tunable vHS and the absence of structural instabilities make CsTi_3Bi_5 a complementary material platform to compare with CsV_3Sb_5 . In CsV_3Sb_5 , the existence of electronic and structural instabilities give rise to various emergent phenomena. However, their coexistence also makes it hard to differentiate the primary driving mechanism for the different phenomena. In CsTi_3Bi_5 , without the interference from the lattice, one can systematically examine the electronic instabilities. For example, the CDW order is absent in pristine CsTi_3Bi_5 [34,35], and no CDW gap is observed in our ARPES measurements (Supplemental Material Fig. S4 [37]). This could be attributed to either

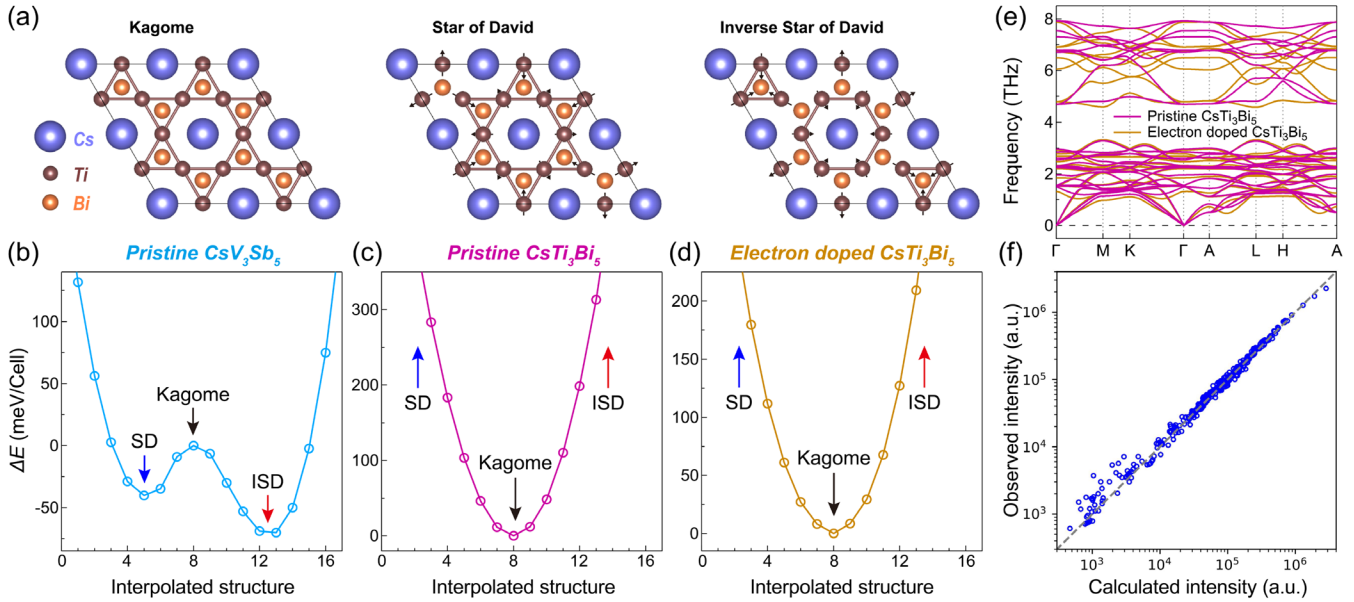


FIG. 4. Calculated total energy profiles, phonon spectra, and x-ray diffraction measurements. (a) The $2 \times 2 \times 1$ supercells for kagome structure, Star of David structure and Inverse Star of David structure. The black arrows indicate the lattice distortion due to the breathing mode. (b)–(d) Total energy as a function of the interpolated structure in pristine CsV_3Sb_5 (b), pristine CsTi_3Bi_5 (c), and electron doped CsTi_3Bi_5 (d). The ΔE stands for the relative total energy with respect to the kagome structure per supercell (36 atoms). (e) Calculated phonon spectra along the high-symmetry directions in pristine CsTi_3Bi_5 (magenta line) and electron doped CsTi_3Bi_5 (orange line). (f) Comparison between the observed x-ray diffraction intensities from 322 indexed Bragg peaks measured at 18 K and the calculation from the crystal structure of CsTi_3Bi_5 with the space group of $P6/mmm$.

the absence of the electronic nesting condition or the absence of the imaginary frequency in the phonon spectra. However, when the vHS is tuned to the vicinity of E_F , the photoemission spectra remain gapless at low temperature (Supplemental Material Fig. S5 [37]). These results indicate that the electronic nesting between vHSs at \bar{M} points alone is insufficient to drive a CDW order in the kagome metal. This point can also be illustrated by the zero-frequency joint density of states [22,46] calculated from the autocorrelation of the measured Fermi surface, where a peak appears at \bar{M} point (nesting between vHSs) in both CsV_3Sb_5 and Cs doped CsTi_3Bi_5 , but disappears in the pristine CsTi_3Bi_5 (see Supplemental Material Figs. S6-7 [37]). In order to understand the origin, we have calculated the charge susceptibility in CsTi_3Bi_5 (see Supplemental Material Fig. S8 [37]). A finite peak does appear at the M point when the Fermi level is at the vHS. However, an unreasonably large Coulomb interaction is required to drive the CDW transition when pure electronic interactions are considered. In this context, the structural instabilities in CsV_3Sb_5 may play an essential role in driving the CDW order. This is also supported by our calculations showing that the CDW transition as a function of doping is determined by the total energy of the system (see Supplemental Material Fig. S9 [37]). Nevertheless, the electronic correlation in CsV_3Sb_5 may contribute to the unconventional behaviors of the CDW orders, although a structural instability seems to be important to trigger the phase transition. On the other hand, nematic order reported

in CsTi_3Bi_5 [47,48] can only be driven by pure electronic interactions. Our DFT calculations and x-ray diffraction measurement illustrate that the lattice of CsTi_3Bi_5 reserves sixfold symmetry [Fig. 4(f) and Supplemental Material, Figs. S10-11 [37]], whereas our polarization dependent ARPES measurements point to the existence of orbital hybridization (Supplemental Material, Figs. S12-13 [37]), echoing the theoretical proposal of a rotational symmetry breaking hybridizations among different orbitals [47,48]. In this context, it would be interesting to further explore how the tunable vHS in CsTi_3Bi_5 would interact with the nematic order and other potential electronic orders in the system.

In summary, we have revealed the electronic structure of pristine and Cs surface doped CsTi_3Bi_5 samples. The Cs deposition induces an overall electron doping to the material, but the energy bands exhibit an orbital dependent movement with doping. Among them, the vHS can be tuned in a large energy range. First-principles calculations demonstrate that the kagome structure remains stable in both pristine and electron doped CsTi_3Bi_5 . These results establish a unique path to disentangle the electronic instability from that of the lattice, and to examine its relationship with the various exotic phenomena in kagome metals.

We thank Y.L. Han, T. Wu, Z. J. Xiang, Z. Y. Wang, X. H. Chen, I. Zeljkovic, and H. Chen for useful discussions. The work at University of Science and Technology of

China (USTC) was supported by the National Natural Science Foundation of China (No. 52273309, No. 12074358, No. 52261135638), the Fundamental Research Funds for the Central Universities (No. WK3510000012, No. WK2030000035), the Innovation Program for Quantum Science and Technology (No. 2021ZD0302802) and the USTC start-up fund. The work at Southwest University was supported by the National Science Foundation of China (Grant No. 11704315). The work at Beijing Institute of Technology was supported by the National Key R&D Program of China (Grants No. 2020YFA0308800, No. 2022YFA1403400), the National Science Foundation of China (Grant No. 92065109), the Beijing Natural Science Foundation (Grants No. Z210006, No. Z190006). This work used resources of the Advanced Light Source, a U.S. Department of Energy (DOE) Office of Science User Facility under Contract No. DE-AC02-05CH11231. This work also acknowledges support by the U.S. Department of Energy, Office of Science, Office of Basic Energy Sciences, Materials Sciences and Engineering Division under Contract No. DE-AC02-05-CH11231 (Quantum materials KC2202). Use of the Stanford Synchrotron Radiation Lightsource, SLAC National Accelerator Laboratory, is supported by the U.S. Department of Energy, Office of Science, Office of Basic Energy Sciences under Contract No. DE-AC02-76SF00515. M.H. and D.L. acknowledge the support of the U.S. Department of Energy, Office of Science, Office of Basic Energy Sciences, Division of Material Sciences and Engineering. The susceptibility simulation used resources of the National Energy Research Scientific Computing Center (NERSC), a U.S. Department of Energy Office of Science User Facility located at Lawrence Berkeley National Laboratory, operated under Contract No. DE-AC02-05CH11231 using NERSC award BES-ERCAP0023810. Y. Y. P. is grateful for financial support from the National Natural Science Foundation of China (No. 11974029). J. H. and Y. L. thank the Analysis & Testing Center at USTC for the support. Z. W. thanks the Analysis & Testing Center at BIT for assistance in facility support.

*These authors contributed equally to this work.

†To whom all correspondence should be addressed.

jfhe@ustc.edu.cn

‡To whom all correspondence should be addressed.

zhiweiwang@bit.edu.cn

- [1] B. R. Ortiz, S. M. L. Teicher, Y. Hu, J. L. Zuo, P. M. Sarte, E. C. Schueller, A. M. M. Abeykoon, M. J. Krogstad, S. Rosenkranz, R. Osborn, R. Seshadri, L. Balents, J. He, and S. D. Wilson, *Phys. Rev. Lett.* **125**, 247002 (2020).
- [2] B. R. Ortiz, P. M. Sarte, E. M. Kenney, M. J. Graf, S. M. L. Teicher, R. Seshadri, and S. D. Wilson, *Phys. Rev. Mater.* **5**, 034801 (2021).
- [3] Q. Yin, Z. Tu, C. Gong, Y. Fu, S. Yan, and H. Lei, *Chin. Phys. Lett.* **38**, 037403 (2021).
- [4] H. Zhao, H. Li, B. R. Ortiz, S. M. L. Teicher, T. Park, M. Ye, Z. Wang, L. Balents, S. D. Wilson, and I. Zeljkovic, *Nature (London)* **599**, 216–221 (2021).
- [5] Z. Liang, X. Hou, F. Zhang, W. Ma, P. Wu, Z. Zhang, F. Yu, J.-J. Ying, K. Jiang, L. Shan, Z. Wang, and X.-H. Chen, *Phys. Rev. X* **11**, 031026 (2021).
- [6] H. Li, T. T. Zhang, T. Yilmaz, Y. Y. Pai, C. E. Marvinney, A. Said, Q. W. Yin, C. S. Gong, Z. J. Tu, E. Vescovo, C. S. Nelson, R. G. Moore, S. Murakami, H. C. Lei, H. N. Lee, B. J. Lawrie, and H. Miao, *Phys. Rev. X* **11**, 031050 (2021).
- [7] B. R. Ortiz, S. M. L. Teicher, L. Kautzsch, P. M. Sarte, N. Ratcliff, J. Harter, J. P. C. Ruff, R. Seshadri, and S. D. Wilson, *Phys. Rev. X* **11**, 041030 (2021).
- [8] F. H. Yu, D. H. Ma, W. Z. Zhuo, S. Q. Liu, X. K. Wen, B. Lei, J. J. Ying, and X. H. Chen, *Nat. Commun.* **12**, 3645 (2021).
- [9] Y. Song, T. Ying, X. Chen, X. Han, X. Wu, A. P. Schnyder, Y. Huang, J.-G. Guo, and X. Chen, *Phys. Rev. Lett.* **127**, 237001 (2021).
- [10] B. Q. Song, X. M. Kong, W. Xia, Q. W. Yin, C. P. Tu, C. C. Zhao, D. Z. Dai, K. Meng, Z. C. Tao, Z. J. Tu, C. S. Gong, H. C. Lei, Y. F. Guo, X. F. Yang, and S. Y. Li, *arXiv:2105.09248*.
- [11] Y.-X. Jiang *et al.*, *Nat. Mater.* **20**, 1353 (2021).
- [12] H. Chen *et al.*, *Nature (London)* **599**, 222 (2021).
- [13] L. Nie *et al.*, *Nature (London)* **604**, 59 (2022).
- [14] Y. Xiang, Q. Li, Y. Li, W. Xie, H. Yang, Z. Wang, Y. Yao, and H.-H. Wen, *Nat. Commun.* **12**, 6727 (2021).
- [15] Y. Hu, S. M. L. Teicher, B. R. Ortiz, Y. Luo, S. Peng, L. Huai, J. Ma, N. C. Plumb, S. D. Wilson, J. He, and M. Shi, *Sci. Bull.* **67**, 495 (2022).
- [16] C. Mielke III *et al.*, *Nature (London)* **602**, 245 (2022).
- [17] L. Yu *et al.*, *arXiv:2107.10714*.
- [18] R. Khasanov, D. Das, R. Gupta, C. Mielke III, M. Elender, Q. Yin, Z. Tu, C. Gong, H. Lei, E. T. Ritz, R. M. Fernandes, T. Birol, Z. Guguchia, and H. Luetkens, *Phys. Rev. Res.* **4**, 023244 (2022).
- [19] M. Kang, S. Fang, J.-K. Kim, B. R. Ortiz, S. H. Ryu, J. Kim, J. Yoo, G. Sangiovanni, D. D. Sante, B.-G. Park, C. Jozwiak, A. Bostwick, E. Rotenberg, E. Kaxiras, S. D. Wilson, J.-H. Park, and R. Comin, *Nat. Phys.* **18**, 301 (2022).
- [20] Y. Hu, X. Wu, B. R. Ortiz, S. Ju, X. Han, J. Ma, N. C. Plumb, M. Radovic, R. Thomale, S. D. Wilson, A. P. Schnyder, and M. Shi, *Nat. Commun.* **13**, 2220 (2022).
- [21] Z. Liu, N. Zhao, Q. Yin, C. Gong, Z. Tu, M. Li, W. Song, Z. Liu, D. Shen, Y. Huang, K. Liu, H. Lei, and S. Wang, *Phys. Rev. X* **11**, 041010 (2021).
- [22] S. Cho, H. Ma, W. Xia, Y. Yang, Z. Liu, Z. Huang, Z. Jiang, X. Lu, J. Liu, Z. Liu, J. Li, J. Wang, Y. Liu, J. Jia, Y. Guo, J. Liu, and D. Shen, *Phys. Rev. Lett.* **127**, 236401 (2021).
- [23] H. Tan, Y. Liu, Z. Wang, and B. Yan, *Phys. Rev. Lett.* **127**, 046401 (2021).
- [24] R. Lou, A. Fedorov, Q. Yin, A. Kuibarov, Z. Tu, C. Gong, E. F. Schwier, B. Buchner, H. Lei, and S. Borisenko, *Phys. Rev. Lett.* **128**, 036402 (2022).
- [25] X. Zhou, Y. Li, X. Fan, J. Hao, Y. Dai, Z. Wang, Y. Yao, and H.-H. Wen, *Phys. Rev. B* **104**, L041101 (2021).
- [26] H. Luo *et al.*, *Nat. Commun.* **13**, 273 (2022).

- [27] E. Uykur, B. R. Ortiz, S. D. Wilson, M. Dressel, and A. A. Tsirlin, *npj Quantum Mater.* **7**, 16 (2022).
- [28] Y. Xie, Y. Li, P. Bourges, A. Ivanov, Z. Ye, J.-X. Yin, M. Z. Hasan, A. Luo, Y. Yao, Z. Wang, G. Xu, and P. Dai, *Phys. Rev. B* **105**, L140501 (2022).
- [29] Z. Ye, A. Luo, J.-X. Yin, M. Z. Hasan, and G. Xu, *Phys. Rev. B* **105**, 245121 (2022).
- [30] M. Wenzel, B. R. Ortiz, S. D. Wilson, M. Dressel, A. A. Tsirlin, and E. Uykur, [arXiv:2112.07501](https://arxiv.org/abs/2112.07501).
- [31] Z. Jiang, H. Ma, W. Xia, Q. Xiao, Z. Liu, Z. Liu, Y. Yang, J. Ding, Z. Huang, J. Liu, Y. Qiao, J. Liu, Y. Peng, S. Cho, Y. Guo, J. Liu, and D. Shen, [arXiv:2208.01499](https://arxiv.org/abs/2208.01499).
- [32] Y. Jiang, Z. Yu, Y. Wang, T. Lu, S. Meng, K. Jiang, and M. Liu, *Chin. Phys. Lett.* **39**, 047402 (2022).
- [33] X.-W. Yi, X.-Y. Ma, Z. Zhang, Z.-W. Liao, J.-Y. You, and G. Su, [arXiv:2202.05588](https://arxiv.org/abs/2202.05588).
- [34] H. Yang, Z. Zhao, X.-W. Yi, J. Liu, J.-Y. You, Y. Zhang, H. Guo, X. Lin, C. Shen, H. Chen, X. Dong, G. Su, and H.-J. Gao, [arXiv:2209.03840](https://arxiv.org/abs/2209.03840).
- [35] D. Werhahn, B. R. Ortiz, A. K. Hay, S. D. Wilson, R. Seshadri, and D. Johrendt, *Z. Naturforsch. B online* (2022), [10.1515/znb-2022-0125](https://doi.org/10.1515/znb-2022-0125).
- [36] K. Nakayama, Y. Li, T. Kato, M. Liu, Z. Wang, T. Takahashi, Y. Yao, and T. Sato, *Phys. Rev. X* **12**, 011001 (2022).
- [37] See Supplemental Material at <http://link.aps.org/supplemental/10.1103/PhysRevLett.131.026701> for the details of the theoretical calculations and other supporting information, which includes Refs. [23,28,38–45].
- [38] M. D. Johannes, I. I. Mazin, and C. A. Howells, *Phys. Rev. B* **73**, 205102 (2006).
- [39] G. Kresse and J. Hafner, *Phys. Rev. B* **48**, 13115 (1993).
- [40] G. Kresse and J. Furthmüller, *Comput. Mater. Sci.* **6**, 15 (1996).
- [41] P. E. Blöchl, *Phys. Rev. B* **50**, 17953 (1994).
- [42] J. P. Perdew, K. Burke, and M. Ernzerhof, *Phys. Rev. Lett.* **77**, 3865 (1996); **78**, 1396 (1997).
- [43] S. Grimme, J. Antony, S. Ehrlich, and H. Krieg, *J. Chem. Phys.* **132**, 154104 (2010).
- [44] A. Togo and I. Tanaka, *Scr. Mater.* **108**, 1 (2015).
- [45] Q. S. Wu, S. Zhang, H. F. Song, M. Troyer, and A. A. Soluyanov, *Comput. Phys. Commun.* **224**, 405 (2018).
- [46] Z. Jiang, Z. Liu, H. Ma, W. Xia, Z. Liu, J. Liu, S. Cho, Y. Yang, J. Ding, J. Liu, Z. Huang, Y. Qiao, J. Shen, W. Jing, X. Liu, J. Liu, Y. Guo, and D. Shen, [arXiv:2212.02399](https://arxiv.org/abs/2212.02399).
- [47] H. Yang *et al.*, [arXiv:2211.12264](https://arxiv.org/abs/2211.12264).
- [48] H. Li, S. Cheng, B. R. Ortiz, H. Tan, D. Werhahn, K. Zeng, D. Jorhendt, B. Yan, Z. Wang, S. D. Wilson, and I. Zeljkovic, [arXiv:2211.16477](https://arxiv.org/abs/2211.16477).